Potassium-selective block of barium permeation through single KcsA channels

Kene N. Piasta,[1,2] Douglas L. Theobald,[1] and Christopher Miller[1,2]

[1]Department of Biochemistry and [2]Howard Hughes Medical Institute, Brandeis University, Waltham, MA 02454

Ba^{2+}, a doubly charged analogue of K^+, specifically blocks K^+ channels by virtue of electrostatic stabilization in the permeation pathway. Ba^{2+} block is used here as a tool to determine the equilibrium binding affinity for various monovalent cations at specific sites in the selectivity filter of a noninactivating mutant of KcsA. At high concentrations of external K^+, the block-time distribution is double exponential, marking at least two Ba^{2+} sites in the selectivity filter, in accord with a Ba^{2+}-containing crystal structure of KcsA. By analyzing block as a function of extracellular K^+, we determined the equilibrium dissociation constant of K^+ and of other monovalent cations at an extracellular site, presumably S1, to arrive at a selectivity sequence for binding at this site: Rb^+ (3 µM) > Cs^+ (23 µM) > K^+ (29 µM) > NH_4^+ (440 µM) >> Na^+ and Li^+ (>1 M). This represents an unusually high selectivity for K^+ over Na^+, with $|\Delta\Delta G^0|$ of at least 7 kcal mol^{-1}. These results fit well with other kinetic measurements of selectivity as well as with the many crystal structures of KcsA in various ionic conditions.

INTRODUCTION

The ability of K^+ channels to strongly favor permeation of K^+ over Na^+ lies at the heart of innumerable physiological processes. The appearance almost 15 years ago of the x-ray crystal structure of KcsA, the first high-resolution view of a K^+ channel (Doyle et al., 1998), elevated discourse on ion selectivity mechanisms from prescient cartoons (Hodgkin and Keynes, 1955; Bezanilla and Armstrong, 1972; Neyton and Miller, 1988a) to the close-up chemistry of ion coordination. KcsA, a bacterial protein, contains a canonical K^+ selectivity filter identical in sequence and structure to those now known in many molecular families of K^+ channels throughout the biological universe. This structure, formed along the central axis of the homotetrameric protein, is essentially a narrow tunnel 15 Å in length, lined by 20 oxygen atoms that form four K^+-binding sites, numbered S1–S4 from extracellular to intracellular (Fig. 1). Under physiological conducting conditions, two of these sites on average are occupied by K^+ (Zhou and MacKinnon, 2003). The striking geometrical match of these sites to the diameter of a dehydrated K^+ ion, 2.7 Å, immediately suggested that K^+ selectivity emerges from "snug-fit" of the preferred ion (Doyle et al., 1998; Lockless et al., 2007), a mechanism proposed long ago (Bezanilla and Armstrong, 1972), when K^+ channels were viewed merely as bio-electronic circuit elements of unknown molecular character. This mechanism posits a thermodynamic tug-of-war for cations between protein and aqueous solution; while the protein mimics the hydration shell of K^+, its presumed rigidity prevents the filter from collapsing inward to similarly embrace the smaller Na^+ ion as solvent water is free to do. Thus, a K^+ ion diffusing up to the channel perceives the selectivity filter as an isoenergetic, aquomimetic diffusion pathway, whereas a Na^+ ion is confronted by large kinetic barriers to entry and transit.

Despite the simplicity, elegance, and aesthetic appeal of the snug-fit picture, the mechanism of K^+ channel selectivity has elicited a many-voiced debate over the past few years (see Andersen, 2011, and related papers for a recent perspective on this subject). With snug-fit in a rigid selectivity filter at one extreme versus a loose, dynamic filter whose selectivity reflects intrinsic chemistry of the carbonyl group at the other (Noskov and Roux, 2007; Roux, 2010), additional proposals based on ionic coordination numbers (Varma et al., 2008) or simply the number of ion-binding sites along the selectivity filter (Derebe et al., 2011) have been offered. Matters are further confounded by a gaggle of computational conclusions that have variously assigned K^+-selective electrophysiological characteristics of KcsA to different sites in the filter, or have even claimed certain sites to be Na^+ selective (Åqvist and Luzhkov, 2000; Bernèche and Roux, 2001; Thompson et al., 2009; Egwolf and Roux, 2010; Cheng et al., 2011).

A fundamental limitation in distinguishing these mechanisms is the scarcity of experimental selectivity measurements at thermodynamic equilibrium for specific

Correspondence to Christopher Miller: cmiller@brandeis.edu

Abbreviations used in this paper: BK, Ca^{2+}-activated K^+; PDF, probability density function.

The Rockefeller University Press $30.00
J. Gen. Physiol. Vol. 138 No. 4 421–436
www.jgp.org/cgi/doi/10.1085/jgp.201110684

ion-binding sites. Such data are needed to constrain computations by known values of Gibbs free energy along the filter. Conventional electrophysiological metrics of selectivity, such as single-channel conductance or bi-ionic reversal potential, are straightforward and directly relevant to biological function but problematic in linking experiment to computation, as they are kinetic properties reflecting complex mixtures of energies involving the entire collection of sites in the filter and the transition-state barriers between them. Direct equilibrium ion binding to KcsA by isothermal calorimetry (Lockless et al., 2007) shows good correspondence with electrophysiological measurements but does not distinguish individual sites within the filter, and also includes effects of linked conformational rearrangements. A recent solid-state NMR study providing a first view of site-specific K^+ binding in KcsA (Bhate et al., 2010) concluded that K^+ begins to occupy the filter in the 10-µM concentration range and provides an important experimental basis for future selectivity studies.

This study is aimed at gaining an enhanced view of ion binding to a specific location—the extracellular end—of the KcsA selectivity filter. We apply a method previously introduced with mammalian Ca^{2+}-activated K^+ (BK) channels for determining ion binding to pore sites at thermodynamic equilibrium (Neyton and Miller, 1988a,b). This approach exploits block of single channels by Ba^{2+} ion; with a crystal radius precisely equal to that of K^+, Ba^{2+} masquerades as a divalent K^+ ion and thus, in natural agreement with the snug-fit proposal (Lockless et al., 2007), specifically and strongly blocks K^+ channels. As we show here, Ba^{2+} block allows analysis of ionic interactions within the ion-occluded selectivity filter to quantify equilibrium binding constants of K^+ and its analogues. We focus on the extracellular region of KcsA and demonstrate the extreme K^+ selectivity of the S1/S2 sites, with exceptionally strong selectivity for binding of K^+, Rb^+, Cs^+, and NH_4^+ over Na^+ and Li^+.

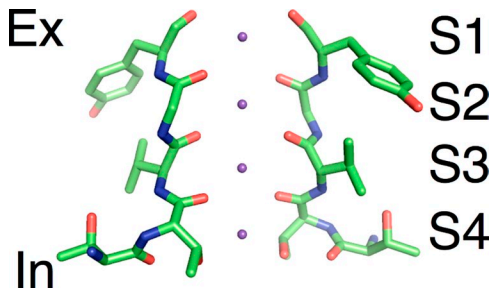

Figure 1. K^+-binding sites in KcsA selectivity filter. Small purple spheres mark locations of sites where K^+ ions appear in crystal structures of the KcsA selectivity filter, shown as stick models of T74-Y78 of two opposing subunits of the tetramer. Sites are numbered S1–S4 from external to internal sides of the filter (deposited in the Protein Data Bank under accession no. 1K4C).

MATERIALS AND METHODS

Materials

Escherichia coli polar lipid (EPL), 1-palmitoyl,2-oleoyl phosphatidylethanolamine (POPE), and 1-palmitoyl-2-oleoyl-*sn*-glycero-3-phospho-(1′-rac-glycerol) (POPG) were purchased from Avanti Polar Lipids, Inc. Decylmaltoside (DM) was purchased from Affymetrix. Ultra-pure LiCl, NaCl, RbCl, CsCl, and NH_4Cl were purchased from Alfa Aesar. *N*-methylglucamine (NMG) contributed <5 µM K^+ to the recording solutions.

Biochemical procedures

The E71A KcsA mutation was constructed with the Quickchange Site-Directed Mutagenesis kit (Agilent Technologies) and confirmed by DNA sequencing. N-terminal hexahistidine-tagged KcsA-E71A protein was expressed in *E. coli* BL21 (DE3) cells, extracted in 100 mM KCl, 50 mM DM, and 20 mM tris-HCl, pH 7.5, and purified by cobalt-affinity (Talon; BD) and size-exclusion chromatography (Superdex 200; GE Healthcare). The final protein preparation was collected at 2–4 mg/ml in 100 mM KCl, 5 mM DM, and 50 mM tris-HCl, pH 7.5.

Liposomes reconstituted with KcsA-E71A were formed from a micellar solution of 35 mM CHAPS, 20 mg/ml EPL, and 10–40 µg protein/ml in reconstitution buffer (200 mM KCl and 10 mM MOPS, pH 7.0). The low protein/lipid ratio favors incorporation of single channels into the electrical recording system. The protein–lipid mix was dialyzed against reconstitution buffer 18–20 h at room temperature with three changes of solution, and the resulting suspension of channel-bearing liposomes was frozen at −80°C in 50-µl aliquots. For a day's work, an aliquot was diluted with 50 µl of 1.5 M KCl, refrozen, thawed, and sonicated for 5–10 s in a cylindrical bath sonicator.

Single-channel recording

Single channels were recorded at 21 ± 1°C in a horizontal planar bilayer system with two aqueous chambers separated by a 80-µm-thick partition hand-crafted from overhead transparency film (Heginbotham et al., 1999); bilayers were formed from POPE/POPG (7.5:2.5 mg/ml in *n*-decane) on an ∼50-µm hole punched with a conical-tip butterfly-mounting pin (BioQuip Products, Inc.) and shaved smooth with a surgical scalpel. Unless specified otherwise, the "internal" aqueous chamber contained 195 mM KCl and 5 mM KOH, adjusted to pH 4.0 with succinic acid, and the "external" chamber contained the test monovalent cation (Cl^- salt) and 10 mM MOPS, adjusted to pH 7.0 with NMG base, as well as NMG-Cl at a concentration to maintain ionic strength at 105 mM. The pH gradient used here ensures that channels appear in the correct biological orientation, with cytoplasmic and extracellular sides of the protein facing the internal and external solutions, respectively (Heginbotham et al., 1999). Voltage, corrected for junction potential (∼5 mV), is reported according to the electrophysiological convention, with the external side defined as ground. Current was recorded via an amplifier (Axopatch-200B; Molecular Devices), with signals sampled at 10 kHz after low-pass filtering (eight-pole Bessel, 0.75–1-kHz corner frequency).

Single-channel recordings were obtained by squirting 0.5 µl of a liposome suspension onto the internal side of the bilayer and waiting 2–5 min, according to the patience of the investigator. Channel insertion was monitored and voltage controlled remotely by iPhone. Upon appearance of a channel (at 45–50 mV) as an ∼6-pA current step exhibiting submillisecond closures, chambers were perfused with fresh solutions. After recording for ∼3 min to confirm proper channel characteristics, 30–60 µM $BaCl_2$ was stirred into the internal solution. Recordings were checked for stationarity and idealized using Clampfit software, and dwell-time distributions were fit to multiple exponential components (after correction for an egregious Clampfit 9.2 bug in log-binning).

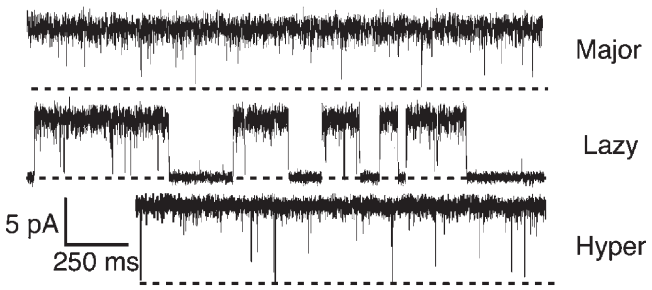

Figure 2. Personality quirks in KcsA-E71A. Illustrative recordings are shown for three clearly distinguishable single-channel personalities observed here, with names indicated. Dashed lines mark zero-current level, here and throughout.

Open-time distributions fit well to single exponentials. Spontaneous closings contributed a submillisecond component to the triple-exponential distributions for nonconducting times in the presence of Ba^{2+}; correction of these distributions for missed events because of the rapid spontaneous closings was unnecessary, as the analysis here is concerned only with the Ba^{2+}-induced block events. Bayesian analysis of dwell times (described in Appendix A) was performed with home-written software.

We encountered several experimental complications in obtaining blocks under the special condition of external Ba^{2+} and zero external K^+. In this condition, the on-rate for Ba^{2+} from the external side is low ($\sim$100 $M^{-1}s^{-1}$), and so high concentrations (1 mM) must be used to obtain a practicable frequency of block events; Ba^{2+} cannot be increased further, because above this concentration, the channels become intractably noisy, and even with 1 mM Ba^{2+}, it was necessary to filter the records at 300 Hz to accurately analyze the blocked intervals. A further complication arose from spontaneous inactivation events, which, although extremely rare in the mutant used here, are not entirely absent (Chakrapani et al., 2011); these events contribute a small fraction of nonconducting times that, with $\sim$50-ms average duration, are easily separated from the Ba^{2+} blocks ($\sim$5 ms). These spontaneous inactivation events are noticeable only with external Ba^{2+}; they are so infrequent ($\sim$0.05 s^{-1}) that they do not taint any of the recordings with internal Ba^{2+}.

Selection of channels for recording and analysis

Despite the high purity and chromatographic homogeneity of our protein preparations, we routinely observed KcsA-E71A channels with three distinct behaviors, denoted "major," "lazy," and "hyper" (Fig. 2). The major channel, of $\sim$6.5 pA amplitude at 50 mV and excess open-channel noise, exhibits high open probability (0.95–0.99), as originally described for this mutant (Cordero-Morales et al., 2006), with closings on the 0.1–1-ms timescale. The lazy channel, of identical amplitude and open-channel noise, displays an additional set of 100-ms-timescale closings leading to open probability below 0.8. The hyper channel amplitude is 8–9 pA, with high open probability and low open-state noise. We have observed channels switch among these behaviors over the minutes-to-hours duration of our experiments, but such events are extremely rare. With proteoliposome preparations stored for less than 1 month, the major channel is observed $\sim$80% of the time, but this frequency decreases, and the lazy and hyper channels become more prevalent, as preparations age in the freezer. We have no explanation for this diversity in channel personality, which recalls a recent report of similar behaviors in wild-type KcsA (Chakrapani et al., 2011). The major channel was selected for all experiments reported here.

RESULTS

This study requires long steady-state recordings of single KcsA channels blocked by Ba^{2+} ions. However, a robust inactivation process (Gao et al., 2005; Cordero-Morales et al., 2006) renders wild-type KcsA unsuitable for such

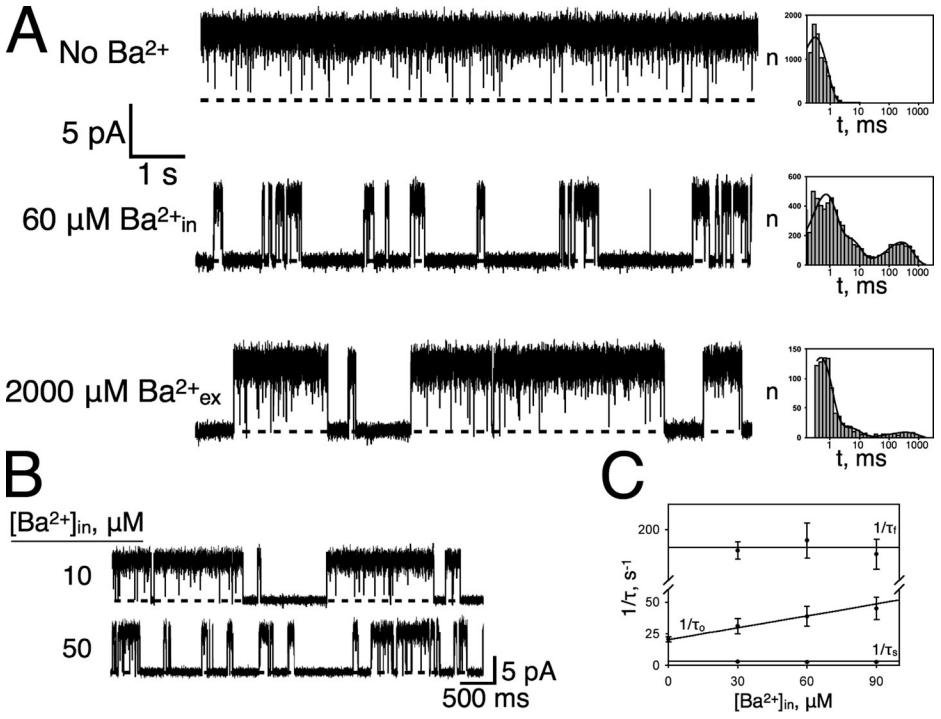

Figure 3. Ba^{2+} block of KcsA-E71. Single-channel recordings were collected at 50 mV with 200 mM of internal K^+/20 mM of internal K^+, with or without Ba^{2+} as indicated. (A) Ba^{2+} blocks from either side of the membrane. Nonconducting dwell-time histograms (log-binned) are shown in each condition, along with exponential fits. Time constant for zero Ba^{2+} is 0.4 ms; time constants of triple-exponential fits for internal Ba^{2+} are 0.9, 6, and 370 ms, and for external Ba^{2+} are 0.3, 5, and 350 ms, respectively. (B and C) Bimolecular behavior of Ba^{2+} block. Representative recordings at two concentrations of internal Ba^{2+} are shown along with plots of inverse time constants for unblocked times ($1/\tau_o$) and fast and slow block times. Second-order rate constant for Ba^{2+} association derived from slope of unblocked-time data is 2.9×10^5 $M^{-1}s^{-1}$.

work. For this reason, we exploit an inactivation-removed mutant, E71A, that retains the channel's acid-activated, voltage-dependent gating and K^+-selective conduction properties (Cordero-Morales et al., 2006; Thompson et al., 2008). When incorporated into planar lipid bilayers under maximal activation conditions (internal 200 mM $[K^+]_{in}$, pH 4, external 20 mM $[K^+]_{ex}$, pH 7), single KcsA-E71A channels display open probability of ~0.98, stable up to 3 h at 50 mV, with submillisecond closings (Fig. 3 A), which Chakrapani et al. (2011) have argued reflect conformational fluctuations of the selectivity filter.

Bimolecular Ba^{2+} block by slow permeation

Ba^{2+} added to either side of the membrane induces a novel set of nonconducting events 10–1,000-fold longer lived than the spontaneous closings (Fig. 3 A). We refer to these events as "Ba^{2+} blocks," which are easily distinguished from the brief closings. Block times follow a double-exponential probability density function (PDF), with fast and slow time constants (τ_f, τ_s) of ~5 and 300 ms under these recording conditions. Block-time distributions are independent of Ba^{2+} concentration, whereas conducting dwell times follow single-exponential distributions whose inverse time constants vary linearly with $[Ba^{2+}]$ (Fig. 3 C). These characteristics are expected for a bimolecular mechanism in which each nonconducting event represents a single Ba^{2+} ion entering the pore and physically blocking K^+ current while it resides there (Vergara and Latorre, 1983; Miller, 1987). Moreover, the block times are the same regardless of the side of Ba^{2+} addition; this fact establishes that Ba^{2+} accesses the same blocking sites from either side of the channel and hence is able to traverse the entire pore, as is well-known for Ba^{2+} block of other K^+ channels. Block is specific to Ba^{2+}; neither Sr^{2+} nor Ca^{2+} produces discernible blocking events (not depicted).

A two-site blocking mechanism

Ba^{2+}-soaked crystal structures of wild-type KcsA in the absence of K^+ show two distinct Ba^{2+} densities within the selectivity filter: an inner site coincident with the S4 K^+ site near the internal end of the selectivity filter, and a deeper site close to S2 (Lockless et al., 2007). We suppose that the double-exponential block-time distributions observed with the E71A mutant reflect these two sites. Furthermore, the strictly bimolecular blocking behavior confirms the crystallographic inference that Ba^{2+} ions do not simultaneously occupy both sites. Thus, once inside the selectivity filter, a single Ba^{2+} ion alternates back and forth between S4 and S2 before leaving the channel to terminate the block event. This picture with two sequential Ba^{2+} block sites is embodied in Fig. 4, which explicitly represents Ba^{2+} entering the channel from the internal side to initiate block at S4. The scheme allows that Ba^{2+} may leave the channel by either of two routes: by dissociation back to the internal side from which it entered ("b route"), or by permeation through the channel to the external Ba^{2+}-free side ("z route"). Thus, Ba^{2+} is formally a conducting ion like its monovalent isostere K^+, but with $\sim 10^7$-fold slower dissociation kinetics. Similar two-site schemes are well established for Ba^{2+} block of BK and K_v channels (Sohma et al., 1996; Harris et al., 1998).

The kinetic scheme above, which includes the submillisecond closings, demands a triple-exponential distribution for the nonconducting dwell times, from which the Ba^{2+}-induced blocks—the part of the distribution in which we are interested—may be readily dissected. These follow a double-exponential PDF, with three independent parameters: the fast and slow time constants τ_f and τ_s, and either of the corresponding amplitudes a_f and a_s, as has been treated previously in detail (Colquhoun and Hawkes, 2009a):

$$p(t) = a_f e^{-t/\tau_f} + a_s e^{-t/\tau_s} \quad (1a)$$

$$\tau_f = \frac{b+c+d+z}{2(bd+bz+cz)}\left(1-\sqrt{1-4\frac{bd+bz+cz}{(b+c+d+z)^2}}\right) \quad (2a)$$

$$\tau_s = \frac{b+c+d+z}{2(bd+bz+cz)}\left(1+\sqrt{1-4\frac{bd+bz+cz}{(b+c+d+z)^2}}\right) \quad (2b)$$

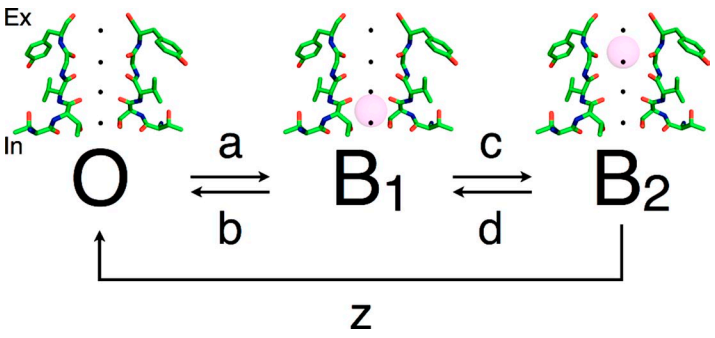

Figure 4. Two-site sequential blocking scheme. The three pertinent states in our kinetic blocking scheme are shown, along with cartoons illustrating Ba^{2+} (purple circles) in positions observed in KcsA and K^+ sites as small black circles (Protein Data Bank accession no. 2ITD). "O" represents the unblocked conducting channel, and B_1 and B_2 are the two blocked states postulated from the two Ba^{2+}-induced components of the nonconducting dwell-time distributions. The scheme refers to internal Ba^{2+}conditions, with z representing irreversible Ba^{2+} exit to the Ba^{2+}-free external side.

$$a_f = \frac{b^2 + bc - b/\tau_s - cz}{(\tau_s - \tau_f)(bd + bz + cz)} \quad (3a)$$

$$a_s = \frac{b/\tau_f + cz - b^2 - bc}{(\tau_s - \tau_f)(bd + bz + cz)} \quad (3b)$$

Also note the useful relations:

$$a_f + a_s = b \quad (4a)$$

$$a_f\tau_f + a_s\tau_s = 1 \quad (4b)$$

$$\frac{1}{\tau_f} + \frac{1}{\tau_s} = b + c + d + z \quad (4c)$$

$$\frac{1}{\tau_f\tau_s} = bd + bz + cz \quad (4d)$$

Henceforth, we will refer solely to block-time distributions, with amplitudes renormalized as in Eqs. 3a and 3b after removing the submillisecond component because of brief closings.

Ba^{2+} block at high external K^+ concentration

The channel's multi-ion single-filing property dictates that Ba^{2+} block kinetics should be sensitive to external K^+ concentration, with internal K^+ held fixed. At low $[K^+]_{ex}$, both b and z routes are available for Ba^{2+} exit. At very high $[K^+]_{ex}$, however, the z route is occluded because the S1 site, immediately adjacent to the external solution, is always occupied by a K^+ ion. Blocks should therefore lengthen as $[K^+]_{ex}$ increases and the z route closes down according to K^+ occupancy at S1. The recordings of Fig. 5 A confirm this expectation. At zero $[K^+]_{ex}$ (with ionic strength maintained by NMG, an impermeant organic cation), Ba^{2+} blocks are brief (on the order of 10 ms), and the addition of external K^+ (5 mM) lengthens them ~30-fold. This Ba^{2+} trapping, or "lock-in," effect has been previously used with BK and K_v channels (Neyton and Miller, 1988a,b; Harris et al., 1998; Vergara et al., 1999) as a quantitative metric of equilibrium binding of K^+ and other cations to specific locations in the selectivity filter. This analysis, which we adopt here, assumes that the kinetics of K^+ equilibration with the Ba^{2+}-blocked pore is much faster than the kinetics of Ba^{2+} exit; because K^+ conduction operates on an ~10-ns timescale, while Ba^{2+} blocks span milliseconds, we consider this a safe supposition.

At the high K^+ extreme, z = 0 by assumption, and so in this condition, the three unknown rate constants b, c, and d may be determined from the three independent parameters derived from the experimental block-time distribution. As will be shown below, at external K^+ concentrations >1 mM, the z route is fully shut down. At such saturating concentrations, the block-time distribution of the dataset of Fig. 5 B yields b = 75 s^{-1}, c = 87 s^{-1}, and d = 7 s^{-1}, and Table I reports values derived from multiple independent datasets, along with values of the underlying rate constants estimated by a Bayesian analysis. Bayesian analysis also confirms the assumption that z ≈ 0 at high K^+. In this fully locked-in condition at +50 mV, with K^+ mainly occupying S1, Ba^{2+} occupancy prefers S2 over S4 by ~1.5 kcal/mol; this estimate is approximate, as the derived values of c and d show substantial channel-to-channel variation, but the preference for S2 is clear.

Ba^{2+} block at zero external K^+

At the opposite extreme of zero external K^+, with the z route unimpeded, block times are short-lived, as seen above (Fig. 5 A). This condition reveals a novel phenomenon: a nonmonotonic block-time distribution with a clear rising or plateau phase (Fig. 6 A; note linear binning of histogram to reveal this feature). Here, the fast-fraction amplitude is negative, as is expected when z becomes sufficiently large (Eq. 3a); a negative PDF amplitude is a rigorous indicator of irreversible steps in the kinetic scheme (Kijima and Kijima, 1987; Colquhoun and Hawkes, 2009a; Csanády et al., 2010), as occurs here in Ba^{2+} exit to the Ba^{2+}-free external solution. Intuitively, the rising phase appears because with S1 unoccupied,

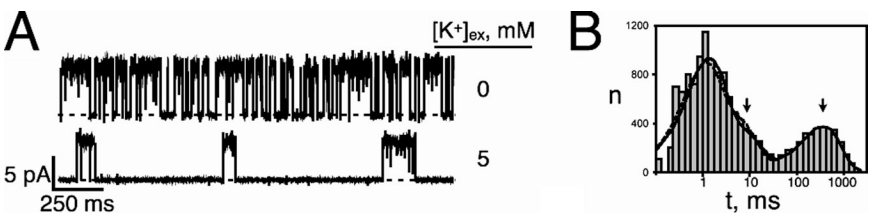

Figure 5. Suppression of Ba^{2+} escape by external K^+. (A) Recordings are shown in the presence of 60 µM of internal Ba^{2+} at zero or 5 mM of external K^+. The presence of external K^+ lengthens block times ~30-fold. (B) Nonconducting time distribution at 5 mM K^+. Solid curve represents double-exponential block-time distribution fit by: a_f and a_s = 75 and 1.5 s^{-1} ; τ_f and τ_s = 6 and 365 ms (time constants for Ba^{2+}-induced blocks are marked by arrows). Dashed curve represents block-time distribution predicted by rate constants derived from Bayesian analysis, using maximum entropy prior.

TABLE I

Ba^{2+} block parameters for KcsA-E71A

K^+	0	3 μM	10 μM	25 μM	50 μM	100 μM	300 μM	500 μM	1 mM	5 mM	20 mM
τ_f (ms)	6 (2)	4.69 (0.04)	7 (1)	—	—	—	—	3.3 (0.5)	4.1 (0.2)	6 (1)	6 (0.3)
τ_s (ms)	15 (1)	17 (1)	20 (1)	31 (1)	34 (2)	47 (3)	96 (2)	146 (5)	179.9 (0.2)	298 (33)	330 (25)
a_f (s^{-1})	−69 (7)	−38 (9)	−38 (15)	—	—	—	—	58 (11)	38 (4)	57 (10)	67 (1)
a_s (s^{-1})	93 (5)	72 (7)	65 (9)	32 (1)	30 (2)	22 (2)	10.4 (0.2)	5.8 (0.3)	4.71 (0.09)	2.5 (0.4)	1.7 (0.2)
b (s^{-1})	24 (6), **44 (2)**	33 (8)	26 (6)	32 (1)	30 (2)	22 (2)	10.4 (0.2)	63 (11)	43 (4)	59 (10)	69 (1), 107 (7)
c (s^{-1})	45, **29 (2)**								175 (12)	127 (27)	79 (4), 95 (5)
d (s^{-1})	18, **7 (6)**								32 (1)	12 (3)	6.8 (0.7), 3.0 (0.3)
z (s^{-1})	175, **204 (6)**								0	0	0, 1.6 (0.1)
Rb^+		1 μM	2 μM	10 μM	20 μM	100 μM	200 μM	1 mM	20 mM		
τ_f (ms)		6 (2)	—	13.7 (0.9)	13.1 (0.6)	11 (2)	11 (1)	9 (2)	4.7 (0.6)		
τ_s (ms)		17 (1)	32 (3)	78 (16)	107 (6)	214 (10)	338 (29)	927 (21)	1,890 (240)		
a_f (s^{-1})		−41 (5)	—	58 (3)	53 (3)	34 (8)	28 (2)	34 (8)	162 (29)		
a_s (s^{-1})		73 (5)	32 (3)1	3.0 (0.9)	2.9 (0.2)	3.1 (0.1)	2.1 (0.2)	0.79 (0.05)	0.15 (0.02)		
b (s^{-1})		32 (9)	32 (3)	61 (4)	56 (3)	37 (8)	31 (2)	34 (8)	162 (29)		
c (s^{-1})								83 (9)	59 (7)		
d (s^{-1})								4.0 (0.5)	0.75 (0.09)		
z (s^{-1})								0	0		
Cs^+		1 μM	10 μM	20 μM	100 μM	1 mM	20 mM				
τ_f (ms)		3.77 (0.05)	—	—	9 (2)	6 (1)	5 (1)				
τ_s (ms)		17.5 (0.4)	21.4 (0.7)	27 (2)	76 (5)	318 (19)	1116 (48)				
a_f (s^{-1})		−41 (13)	—	—	48 (27)	65 (2)	110 (34)				
a_s (s^{-1})		65 (4)	47 (2)	37 (3)	9.5 (0.7)	1.9 (0.1)	0.44 (0.05)				
b (s^{-1})		25 (10)	47 (2)	37 (3)	58 (26)	67 (1)	110 (34)				
c (s^{-1})						96 (22)	96 (3)				
d (s^{-1})						7.9 (0.8)	1.8 (0.2)				
z (s^{-1})						0	0				
NH_4^+		100 μM	500 μM	1 mM	20 mM						
τ_f (ms)		6 (1)	—	—	3 (1)						
τ_s (ms)		17 (4)	28.8 (0.5)	47 (6)	199 (23)						
a_f (s^{-1})		−79 (11)	—	—	125 (42)						
a_s (s^{-1})		87 (10)	34.8 (0.5)	22 (3)	3.1 (0.2)						
b (s^{-1})		7.9 (0.7)	34.8 (0.5)	22 (3)	128 (42)						
c (s^{-1})					181 (42)						
d (s^{-1})					12.8 (0.6)						
z (s^{-1})					0						

Blocking parameters were determined at internal 200 mM K^+ and 50-mV holding voltage, with the indicated concentrations of monovalent cation in the external solution. Time constants and amplitudes were measured by fitting block-time histograms, and rate constants were derived therefrom. Parameters are reported as mean with SEM in parentheses of three to five single-channel datasets in separate bilayers. Dashes indicate components with negligible PDF amplitude, for which block-time PDF was single exponential. Underlined rate constants are mean values (SE in parentheses) determined by Bayesian analysis of four separate datasets for which no assumption about the value of z was made; those in bold refer to Bayesian analysis using prior distribution for z, as described in Appendix A.

most of the blocks terminate via the z route, requiring a delay between the initial binding of Ba^{2+} to S4 and its dissociation from S2 and subsequent passage through the channel. This delay produces a deficit of short blocks—a rising or plateau phase of the distribution. The fast and slow time constants under this condition are 5 and 15 ms, respectively (Table I).

If we would assume that b, c, and d at zero $[K^+]_{ex}$ maintain the values determined above at high K^+, the block-time distribution at zero K^+ would lead immediately to a value for z. But this assumption is unjustified because Ba^{2+} occupancy on S2 and S4 may differ depending on K^+ occupancy at S1. Indeed, if b, c, and d are assumed fixed at their high K^+ values, impossible solutions for z emerge from the measured PDF parameters at $[K^+]_{ex} = 0$ (Eqs. 2a and 2b). We are therefore confronted with an apparently intractable problem: four unknown rate constants to be determined from three measured quantities at zero K^+. In an attempt to obtain rough estimates of the rate constants, we performed a Bayesian analysis of the dwell-time data using a maximum entropy prior distribution that exploits a known upper limit for the rate constants, as described in Appendix A. This analysis produces probability

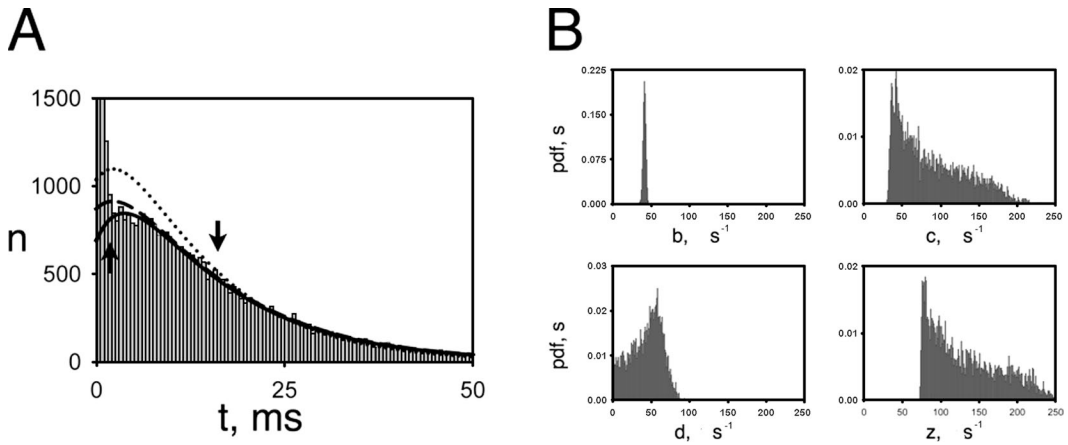

Figure 6. Zero-K^+ block-time distribution with rising phase. (A) Nonconducting dwell-time histogram is shown for a typical dataset with zero external K^+. This histogram is linearly binned to reveal the rising phase of the Ba^{2+}-induced part of the distribution (solid curve, after removal of the Ba^{2+}-independent gating). Parameters of the block-time distribution are: a_f and $a_s = -41$ and $+78\ s^{-1}$; τ_f and $\tau_s = 4$ and 15 ms (marked by arrows). Dotted curve is predicted from the mean values of rate constants derived from Bayesian analysis using a maximum entropy prior, as in Appendix A (b, c, d, and z = 41, 88, 42, and 132 s^{-1}). Dashed curve is predicted by Bayesian analysis using the prior distribution for z shown in Fig. 7 B (b, c, d, and z = 46, 29, 7, and 204 s^{-1}). (B) Distributions of rate constants derived by Bayesian analysis of zero-K^+ dwell times. Parameters from all data are reported in Table I.

distributions for all four rate constants (Fig. 6 B). The distributions are wide, and the rate constant values are correlated with each other (not depicted), because they are underdetermined by the data. The unsatisfactory nature of the analysis is further indicated by the poor fit to the measured dwell-time histogram obtained from the mean values of these distributions (Fig. 6 A, dotted curve).

The situation, however, is not so bleak; we can finesse the difficulty and gain a fourth independent measurement by switching Ba^{2+} to the external side of the channel. Under this condition, all blocks begin in and most terminate from S2, a circumstance that is expected to render both PDF amplitudes positive (and the block-time distribution monotonic). The time constants, however, must be identical according to the kinetic model (Fig. 4) to those obtained from the peaked distribution with internal Ba^{2+}. Either of the PDF amplitudes, which are readily derived from symmetry considerations, thus becomes the fourth independent measurement:

$$\text{external } Ba^{2+}: a_f = \frac{z^2 + dz - z/\tau_s - bd}{(\tau_s - \tau_f)(bz + cz + bd)} \quad a_s = \frac{z/\tau_f - z^2 - zd + bd}{(\tau_s - \tau_f)(bz + cz + bd)}, \tag{5}$$

$$\text{external } Ba^{2+}: z = a_f + a_s = \frac{C_f}{\tau_f} + \frac{(1 - C_f)}{\tau_s}, \tag{6}$$

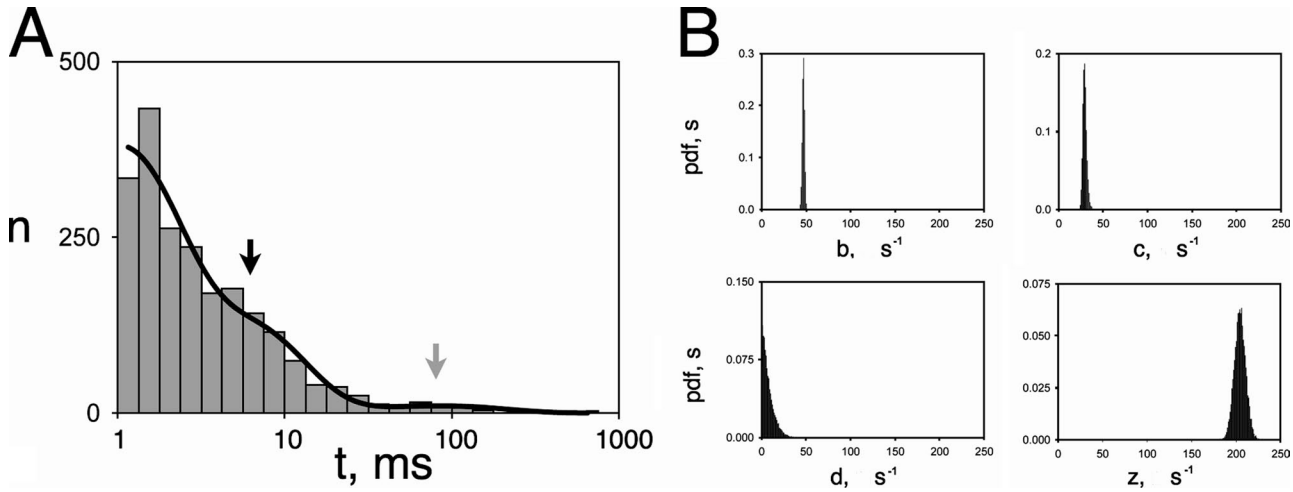

Figure 7. Block by external Ba^{2+} at zero external K^+. (A) Block-time histogram with zero external K^+ and 1 mM of external Ba^{2+}. Solid curve is a triple-exponential fit with a 1-ms component representing heavily filtered spontaneous closings, an 80-ms component (gray arrow) representing rare inactivation events (see Materials and methods), and only a single component for blocks (black arrow), with τ_f constrained by internal Ba^{2+} data to a value of 5.8 ms. (B) Distributions of the rate constants derived from Bayesian analysis of the internal Ba^{2+} data of Fig. 6, now combined with external Ba^{2+} block data. Parameters are reported in Table I.

where C_f is the fraction of fast blocks in the cumulative distribution function.

These expectations are fulfilled, despite experimental difficulties arising under this special external Ba^{2+} zero-K^+ condition (see Materials and methods). The unavoidably low block frequency produces statistically noisy block-time distributions, and consequently the exponential fits are less well defined than with the internal Ba^{2+} data. Nevertheless, the distributions are, as expected, monotonic falling and dominated by the fast fraction of ~6 ms, which makes up at least 90% of the blocks; indeed, the amplitude of the expected 15-ms slow fraction is not significantly different from zero, and the block-time distribution is effectively single exponential under these conditions (Fig. 7 A). For this situation, $z \approx 1/\tau_f$, whose value, 175 s^{-1}, is accurately known from the internal Ba^{2+} data. This allows solution for all four rate constants, b = 25 s^{-1}, c = 49 s^{-1}, d = 18 s^{-1}, and z =175 s^{-1}, as reported in Table I. Bayesian analysis was also applied to the external Ba^{2+} datasets to produce a probability distribution of z. Using this as a prior distribution in a repeat Bayesian analysis of the internal Ba^{2+} data above, we arrive at far cleaner estimates of all four rate constants than before (Fig. 6 B), and derive rigorous estimates of their uncertainties (Fig. 7 B and Table I).

Affinity and selectivity of the trapping site

The above experiments validate a two-site sequential block model and provide a rationale for Ba^{2+} trapping by external K^+. By examining block times as $[K^+]_{ex}$ varies at fixed $[K^+]_{in}$, we can estimate the ion's equilibrium dissociation constant for the external trapping site (Neyton and Miller, 1988b). Block-time distributions at several K^+ concentrations (Fig. 8 A) are shown for data collected using internal Ba^{2+}, and parameters of these distributions for all K^+ concentrations are reported in Table I. As $[K^+]_{ex}$ increases, block times lengthen noticeably at concentrations as low as 10 μM, and the rising phase of the distribution disappears by 25 μM, as K^+ begins to occlude the z route. In the range of 25–500 μM, block times become single exponential as the fast-fraction amplitude rises from its initially negative value through zero to take on negligible values, thus leaving the slow fraction alone to dominate the PDF (Fig. 7 B, dashed region). Above ~1 mM $[K^+]_{ex}$, the distribution is again double exponential but now monotonic falling, as a_f grows increasingly positive. The sign reversal of a_f dictates that Ba^{2+} trapping is best monitored by the time constant of the slow fraction (Fig. 8 B), which dominates the distribution over the entire K^+ concentration range.

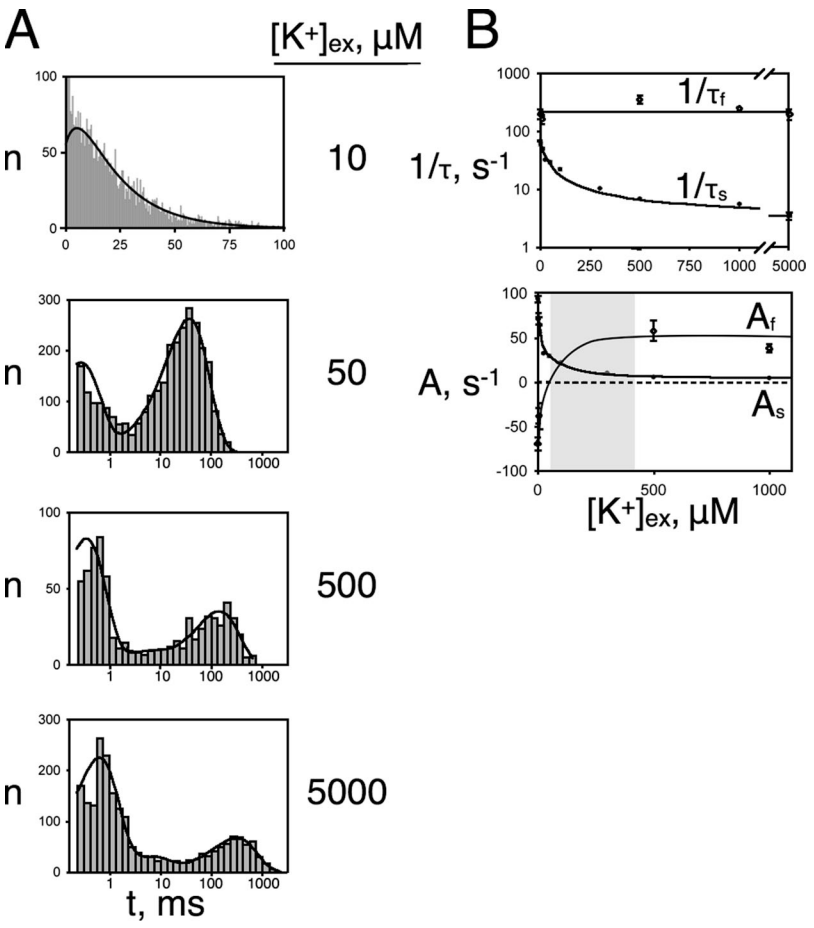

Figure 8. Block of Ba^{2+} permeation by K^+. Ba^{2+} block datasets were recorded as in Fig. 5, at different concentrations of external K^+. (A) Nonconducting time histograms are shown (log-binned except for 10 μM K^+ data, which is binned linearly to show its rising phase). (B) Behavior of fast/slow time constants (top) and amplitudes (bottom) of block-time distributions. Curves have no theoretical meaning, except for the $1/\tau_s$ curve, which plots Eq. 7. Gray shading on the amplitude plot indicates the range of K^+ concentrations where the fast amplitude, in reversing sign, becomes too small to observe and thereby produces a single-exponential block-time distribution.

How should we expect τ_s to vary as external K^+ increases from zero to concentrations at which its effect on block times saturates? We cannot answer this question quantitatively, because we have no model for the K^+ dependence of each individual rate constant in the two-site blocking scheme. A purely empirical analysis, however, can be used to capture the effect of external K^+, as in previous work with BK channels (Neyton and Miller, 1988b; Vergara et al., 1999). We note (Fig. 8 B) that $1/\tau_s$, the slow-fraction Ba^{2+} escape rate, decreases in a graded fashion according to a simple, although theoretically unjustified, single-site binding function:

$$\frac{1}{\tau_s([K^+])} = \frac{1/\tau_s(0) + 1/\tau_s(\infty)\frac{[K^+]}{Ko}}{1+\frac{[K^+]}{Ko}}, \quad (7)$$

where K_o is an empirical "observed" dissociation constant. In general, K_o is not equal to the true K_d but should roughly approximate it, as it directly reflects K^+ occupancy of the trapping site. Calculations based on Eq. 2b show, for instance, that if z alone would decrease with K^+ as above, $1/\tau_s$ would follow a curve similar in shape but with an observed dissociation constant ~1.5-fold larger than the true K_d. Our experimental results (Fig. 8 B) indicate a high K^+ affinity of the lock-in site, with $K_o \approx 30$ μM, close to the 20-μM value found for the BK channel of mammalian skeletal muscle (Neyton and Miller, 1988b; Vergara et al., 1999).

The equilibrium binding selectivity of this site is now straightforwardly determined from analogous experiments with other monovalent cations in the external solution. Recordings in the presence of 100 μM Cs^+, Rb^+, or NH_4^+ (Fig. 9 A) show that these ions also lengthen Ba^{2+} block times. Full Ba^{2+}-trapping curves based on slow-fraction time constants are shown for all ions tested (Fig. 9 B). The pattern of binding selectivity at the external end of the KcsA pore is reminiscent of electrophysiological selectivity metrics among the K^+-like cations for many K^+ channels: $Rb^+ > Cs^+ > K^+ > NH_4^+$. Fig. 9 also illustrates the complete absence of a lock-in effect by Na^+. The addition of 5 mM Na^+, a saturating concentration for K^+, fails to lengthen the block times, and the addition 0.1 mM K^+ on top of this exerts its effect as if no Na^+ were present. Similar experiments with the addition of Na^+ or Li^+ showed no Ba^{2+}-trapping effect whatsoever up to 200 mM (not depicted); this result places a lower limit of ~1.5 M on K_o for Na^+ and Li^+ at the lock-in site, equivalent to a K^+-over-Na^+ selectivity free energy of $\Delta\Delta G^o > 7$ kcal/mol.

DISCUSSION

Two main conclusions emerge from these experiments: Ba^{2+} acts as a slow permeant blocker of KcsA, and the extracellular side of the KcsA selectivity filter binds K^+ with extremely high selectivity over Na^+ or Li^+. These are unsurprising inferences, as it is known from electrophysiological work extending over a half-century that most K^+ channels conduct K^+ with high specificity over other biologically pertinent cations—Na^+, H^+, Mg^{2+}, and Ca^{2+}—and that Ba^{2+}, uniquely among divalent cations, strongly blocks K^+ channels. The utility of the present experiments is that they quantify the standard-state Gibbs free energy of cation transfer from aqueous solution to a specific region within the ion channel's conduction pathway, and thus provide direct experimental links between high-resolution structures and ion-interaction

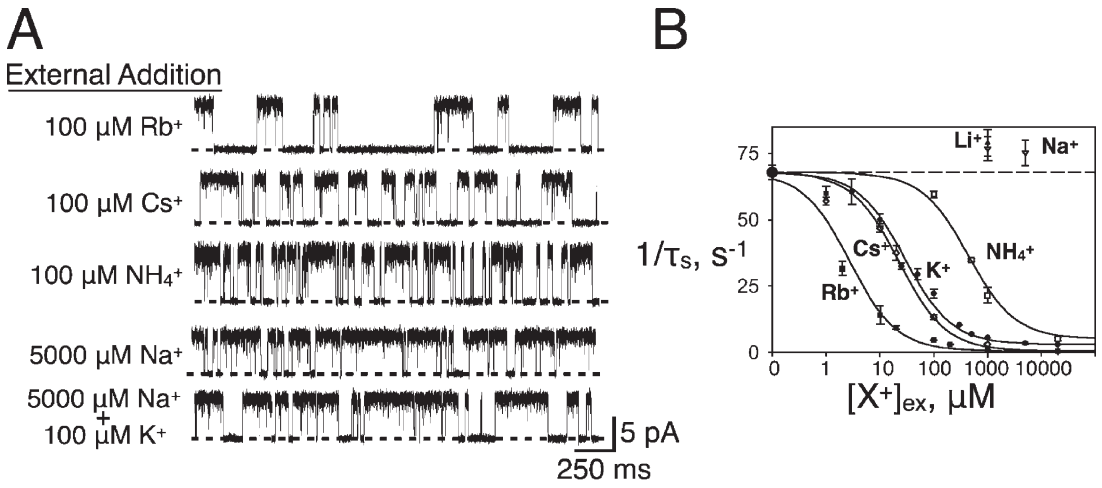

Figure 9. Ion selectivity of external Ba^{2+}-trapping site. Suppression of Ba^{2+} escape by external monovalent cations was performed as in Fig. 8 for K^+. (A) Representative recordings of Ba^{2+} block with external addition of the indicated cations. (B) Titration of inverse slow time constant of block for all cations tested, with data fit by single-site inhibition curves (Eq. 7) constrained to the same zero-K^+ value (solid curves), with half-inhibition constants, in order of affinity: Rb^+ (3 μM), Cs^+ (23 μM), K^+ (29 μM), and NH_4^+ (440 μM).

energetics proposed from computational studies. Although our results are factually straightforward, several questions and ambiguities surrounding them warrant discussion.

Is the E71A mutant a plausible model for wild-type KcsA?

Mechanistic investigations of K^+ channels have frequently required the use of mutations that suppress the various "inactivation" processes necessary for their physiological purposes. The KcsA channel is no exception, as it inactivates strongly after opening (Gao et al., 2005), so that under maximally activated steady-state conditions, it is open <10% of the time (Heginbotham et al., 1999). The Perozo group (Cordero-Morales et al., 2006) described a set of KcsA mutations that suppress inactivation to various degrees, and we chose one of these, E71A, for the experiments here. This inactivation-suppressed mutant displays basic gating and conduction behavior very similar to that of the wild-type channel: activation by low pH and depolarized voltage, K^+ selectivity, and unitary K^+ conductance (Cordero-Morales et al., 2006; Thompson et al., 2008). Moreover, crystal structures of wild-type KcsA and E71A are virtually identical throughout the protein (Chakrapani et al., 2011; Cheng et al., 2011). In our view, these fundamental mechanistic correspondences between wild-type and E71A certify the mutant as a useful model for ion permeation in K^+-selective pores.

However, a few differences between this mutant and wild-type KcsA have been reported. E71A occasionally crystallizes with its selectivity filter in a perplexing "flipped" conformation (Cordero-Morales et al., 2006) that has never been observed in wild-type crystals. In this structure, the backbone carbonyl of Val76 is rotated ∼180° away from the pore, and the amide group of Gly77 points inwards, a circumstance that places electropositive moieties at the level of S2. For this reason, we consider this unusual pore configuration to be nonconducting, although Cheng et al. (2011) have proposed it to be K^+ conducting. A second oddity reported for the E71A mutant is more alarming: permeation by Na^+. Cheng et al. (2011) recently reported $^{22}Na^+$ transport mediated by E71A channels in liposomes. Based on those flux-rate estimates, E71A channels prefer K^+ over Na^+ by a factor of only ∼20, a much lower selectivity than found for wild-type KcsA by ionic fluxes or electrophysiological methods (LeMasurier et al., 2001). However, electrical recording of E71A failed to detect Na^+ current under any conditions. Our own experiments (Appendix B; Fig. B1) demonstrate that the K^+/Na^+ permeability ratio for the E71A mutant, derived by a high-accuracy reversal potential method, is >250. Resolution of these conflicting results awaits future work, but the wild-type–like electrical behavior of E71A gives us confidence in using this mutant as a faithful representative of K^+ channel selectivity filters.

Where are the ion-binding sites?

Our analysis rests on the presumption that Ba^{2+} blocks E71A at the two sites observed in Ba^{2+}-soaked crystals of wild-type KcsA under K^+-free conditions (Lockless et al., 2007). That structure reveals prominent Ba^{2+} densities of roughly equal magnitude near K^+ sites S2 and S4. Of course, Ba^{2+} must transiently visit S3 and S1 during its journey through the selectivity filter, but occupancy on these sites would not, we suppose, be sufficiently favorable to be crystallographically evident. To represent our own recording conditions, it would be desirable to have a crystal structure of E71A in the presence of both Ba^{2+} and K^+. However, we have failed to obtain satisfactory crystal structures of E71A in the presence of Ba^{2+}, with or without K^+, despite the ease of solving Ba^{2+}-free structures of this mutant (not depicted).

The K^+-selective trapping site must lie on the extracellular side of Ba^{2+}, which itself preferentially occupies S2. This is a powerful reason to assign S1 alone for Ba^{2+} trapping, as proposed in analogous work on the BK channel (Vergara et al., 1999). But we should highlight a slight ambiguity on this point. According to the rate constants determined for the two-site blocking scheme (Table I), Ba^{2+} alternates between S2 and S4 on the 10–100-ms timescale during a block interval. Whenever the blocker occupies S2, external K^+ equilibrates exclusively with S1; but when Ba^{2+} resides on S4, K^+ has access to S1, S2, and S3. Because Ba^{2+} tends to favor S2 over S4, the free energy of K^+ binding will be dominated by the chemical properties of S1, with those of S2 and S3 contributing to a lesser degree. Despite this uncertainty, we can confidently assert that S1 must be highly K^+ selective; if it were nonselective, as deduced in a recent computational study (Egwolf and Roux, 2010), external Na^+ should produce significant Ba^{2+} trapping at concentrations comparable to those at which K^+ acts. Clearly, that is not the case. Moreover, it is known (Heginbotham et al., 1999) that although internal Na^+ blocks K^+ current though KcsA, external Na^+ does not, as it would if it had significant affinity in the vicinity of S1. We also note a counterintuitive result regarding the Ba^{2+} sites for which we have no explanation: that the preference of Ba^{2+} for S2 over S4 is even greater at high than at zero K^+, as is evident from the ratio of c to d at the two K^+ concentrations (Table I).

Comparison to other studies of K^+ channels

The Ba^{2+}-trapping maneuver used here on KcsA was originally developed to quantify binding of conducting ions to BK channels from rat muscle (Neyton and Miller, 1988a,b), and was also applied to Shaker-type K_v channels (Harris et al., 1998) before any K^+ channel structures were known. The present results on KcsA generally recapitulate those on BK channels. The external trapping site of BK binds K^+ in the 10-µM range, as with KcsA, and shows the same pattern of ion selectivity for

equilibrium affinity: $Rb^+ > Cs^+ > K^+ > NH^+_4 >> Na^+, Li^+$, a pattern that also appears in conventional electrophysiological selectivity measurements in many classes of K^+ channels (Hille, 2001), including KcsA (LeMasurier et al., 2001). In BK channels, however, Na^+ and Li^+ produce robust Ba^{2+} trapping, with K_d on the order of 10–50 mM, a 1,000-fold selectivity for K^+ over Na^+. The absence, in KcsA, of Ba^{2+} trapping by Na^+ or Li^+, even at concentrations as high as 0.2 M, means that selectivity here is even higher, $>10^5$-fold. Recent work on the MthK channel (Ye et al., 2010) also finds high K^+/Na^+ selectivity at S1 (as well as at S3).

The appearance of the first KcsA structure evoked many computational studies on the ion selectivity of this prototypical pore. From the perspective of experimentalists, these computations have introduced much confusion. Varied theoretical approaches to the KcsA selectivity filter show wildly discrepant results. For example, two molecular dynamics computations from the same research group reported high K^+ selectivity for the S1 site using free energy perturbation methods (Noskov et al., 2004), but little selectivity for the same site using an umbrella sampling approach (Egwolf and Roux, 2010). The difference between these studies is likely a result of sampling density, such that the former examined ions placed inside the carbonyl cage, whereas the latter allowed ions to visit the plane of the carbonyls, a binding configuration also investigated in the S4 region of filter (Thompson et al., 2009). A detailed understanding of the energetic basis of K^+-selective conduction must ultimately rely upon results from molecular dynamics, but until the various computational approaches converge upon consistent results and basic consensus among its practitioners, their utility toward this end will remain doubtful.

The high-affinity problem

Finally, we confess to perplexity regarding a fundamental result: the high affinity of K^+ binding to the selectivity filter, as indicated by Ba^{2+} trapping in the 10-μM range for K^+ and Rb^+. At first blush, this appears to be inconsistent with the channel's electrophysiological behavior. The apparent problem arises from the relationship among rate and dissociation constants for ligand binding to a single site:

$$K_d = k_{off} / k_{on}. \quad (8)$$

Given an experimental equilibrium dissociation constant ($\sim 10^{-5}$ M for K^+), this relationship places an upper limit on the dissociation rate of a bound ligand, as the association rate cannot exceed diffusion limitation ($k_{diff} \sim 10^9\ M^{-1}s^{-1}$):

$$k_{off} < k_{diff} K_d \sim 10{,}000\ s^{-1}. \quad (9)$$

Thus, if K^+ binds to the selectivity filter with micromolar affinity, it must linger there for ∼100 μs before dissociating. However, this is 10^4-fold longer than the nanosecond-timescale residence times for K^+ manifested in typical ∼10-pA single-channel currents. This well-known discrepancy is usually resolved by pointing out that K^+ channels are occupied by several conducting ions simultaneously, so that an ion on a site of intrinsically high affinity becomes destabilized and thus speeded in its exit rate by a second ion nearby in the pore (Hille and Schwarz, 1978; Levitt, 1978; Neyton and Miller, 1988a). Indeed, current models of K^+ channels envision the selectivity filter almost always doubly and occasionally triply occupied at physiological K^+ concentrations on the order of 0.1 M (Morais-Cabral et al., 2001). This idea was corroborated by cunning experiments demonstrating a very slow dissociation rate, $10^4\ s^{-1}$, for the "last" K^+ ion to leave K^+-depleted (presumably singly occupied) Shaker channels (Baukrowitz and Yellen, 1996).

A multi-ion picture like this is quite satisfactory in accounting for K^+ permeation, but it leaves our own results in a quandary. Our experiments focus on K^+ binding to a pore already occupied by a coresident cation, Ba^{2+}, and worse, this cation, being divalent, should be more electrostatically destabilizing than a nearby K^+ ion. The puzzle thus poses itself: if multiple K^+ ions act to mutually destabilize binding 10^4-fold so as to achieve high conduction rates, why does coresidency by Ba^{2+} fail to destabilize K^+ during trapping? Why do we not observe ∼0.1-M K_d values for Ba^{2+} trapping by K^+? One possibility is that Ba^{2+} on its blocking sites somehow perturbs the structure or dynamics of the K^+ site at S1, altering its chemistry to raise its intrinsic affinity to values far greater than under K^+ conduction conditions. This idea—little more than desperate handwaving—is undermined by two experimental facts: (1) Ba^{2+} does not alter the selectivity filter structure of wild-type KcsA (at least to the extent visible at 2.7-Å resolution); and (2) regardless of absolute affinities, the selectivity among group IA cations faithfully reprises the various classical selectivity indicators determined electrophysiologically on the conducting pore.

This problem, which has been staring the field in the face for almost 25 years, thus remains unresolved. Perhaps computational approaches, once they converge to reliability, will accurately address models involving high-charge densities in narrow pores to comprehend at a deeper level the chemical underpinnings of the remarkable and biologically essential selectivity of K^+ channels.

Appendix A: Bayesian analysis of Ba^{2+} block

Advantages of Bayesian methods for single-channel analysis

The object of Bayesian inference is to provide a probability distribution for the parameters of a model, given the observed data (Bernardo and Smith, 1994; Gelman, 2004;

Lee, 2004). The method is based on Bayes's theorem, which expresses the probability of the parameters given the data $p(\theta|x)$ in terms of the likelihood—the probability of the data given the parameters $p(x|\theta)$—and additional information about the parameters expressed as a "prior" distribution $p(\theta)$:

$$p(\theta|x) = p(x|\theta)p(\theta) / A, \quad \text{(A1)}$$

where A is a dimensionless normalization factor.

Relative to classical and likelihood statistics, Bayesian methodology offers many favorable features, of which four of the most relevant for the present analysis are listed below.

(1) Bayesian analysis provides a complete distribution for the parameters of a model, including direct measures of uncertainty. The posterior probability distribution provides a measure of the uncertainty of a parameter estimate, as well as the shape of that uncertainty (which may be represented by a nonsymmetric, skewed, or even multimodal distribution).

(2) Bayesian methodology can incorporate pertinent prior information, in addition to the information given by the data at hand. Previous experiments in different systems or with different experimental setups may provide useful information for constraining realistic parameter values in the present experiment.

(3) Bayesian methodology elegantly handles complex, multi-parameter models without invoking ad hoc techniques. In Bayesian analyses nuisance parameters can simply be integrated out to give a marginal distribution of a parameter that is independent of the others.

(4) Bayesian methods provide solutions for underdetermined systems, which are generally intractable using classical methods. As long as valid priors are specified, Bayes's theorem provides a valid posterior distribution, which may have large uncertainty yet still retain useful information about the unknown parameters.

Application to Ba^{2+} block of KcsA-E71A

Our application of Bayesian methodology to single-channel analysis differs substantially from earlier treatments (Gin et al., 2009; Rosales, 2004; Siekmann et al., 2011). Rather than using hidden Markov models to directly fit the single-channel data (comprising a specific sequence of openings and closings), we use a Bayesian Markov chain Monte Carlo algorithm to infer the rate parameters of our models from the individual distributions of conducting and nonconducting dwell times.

Full five-state scheme with two gating states

For the full Bayesian analysis, we generally assume a five-state scheme with an open state *O*, two block states B_1 and B_2, and two gating states, one extremely fast *C* (the spontaneous closings) and one very slow *I* (the residual rare inactivations). For the internal Ba^{2+} experiments, the B_2 to *O* transition is irreversible, whereas for the external Ba^{2+} experiments, the B_1 to *O* transition is irreversible.

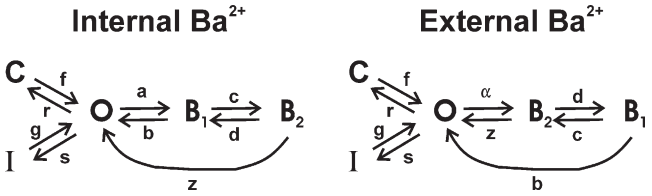

(SCHEME 1)

Likelihood function for five-state scheme

Although the five-state scheme may at first appear rather complicated, inference is greatly simplified by performing two experiments on each channel, one without Ba^{2+} and one with Ba^{2+} added to one side. The no-Ba^{2+} experiments give an independent measurement of the f, r, g, and s rate constants involving only three states in which microscopic reversibility can be assumed. This results in four different datasets from two experiments: openings and closings without Ba^{2+}, and openings and closings with Ba^{2+}. The full likelihood function $p(t|\theta)$ (where *t* is the dwell time and θ is a vector of nine independent rate constants) is thus the product of four PDFs, each with its own independent dataset:

$$p(t|\theta) = p(t|\theta)_{C,Ba}\, p(t|\theta)_{O,Ba}\, p(t|\theta)_{C}\, p(t|\theta)_{O}, \quad \text{(A2)}$$

For a dataset of multiple dwell times (a vector **t** of *N* dwell times), the full joint likelihood function is simply the product of the likelihood for the individual dwell times:

$$p(\mathbf{t}|\theta) = \Pi p(t|\theta), \quad \text{(A3)}$$

where the product is taken over all *N* observed dwell times.

In the following sections, we give expressions for each of these four PDFs.

PDF for closings with Ba^{2+}

The PDF for the Ba^{2+} blocks can be derived using the Q-matrix method as described previously (Colquhoun and Hawkes, 2009a,b), resulting in a quadruple exponential PDF:

$$p(t|\theta)_{C,Ba} = a_f e^{-t/\tau_f} + a_s e^{-t/\tau_s} + a_1 e^{-t/\tau_1} + a_2 e^{-t/\tau_2}, \quad \text{(A4)}$$

where τ_f and τ_s are given in the main text, Eq. 2, and

$$\tau_1 = 1/f \quad \text{(A5a)}$$

$$\tau_2 = 1/g \quad \text{(A5b)}$$

For the internal Ba^{2+} scheme, the amplitudes a_f and a_s are given in the main text, Eqs. 3a and 3b, and

$$a_1 = rf / (a + r + s) \tag{A6a}$$

$$a_2 = sg / (a + r + s) \tag{A6b}$$

PDF for openings with Ba^{2+}

The PDF for openings with Ba^{2+} is a single exponential. For the internal Ba^{2+} scheme,

$$p(t \mid \theta)_{O,Ba} = (a + r + s)e^{-(a+r+s)t}. \tag{A7}$$

PDF for closings or openings without Ba^{2+}

$$p(t \mid \theta)_C = \left(rf / (r + s)\right)e^{-ft} + \left(sg / (r + s)\right)e^{-gt} \tag{A8a}$$

$$p(t \mid \theta)_O = (r + s)e^{-(r+s)t} \tag{A8b}$$

With some channels, the very rare inactivated state *I* was not observed. For these channels, a four-state model was used for inference, in which the g and s rate constants were fixed at zero, with obvious modifications to each of the PDFs. The above relations all pertain to the internal Ba^{2+} scheme. Analogous PDFs for the external Ba^{2+} scheme are obtained by exchanging appropriate rate constants (b<=>z, c<=>d, and a=>α).

Filtered data treated as missing data

Low-pass filtering effectively results in missing events in the dwell-time recordings. We treat these missed events as left-truncated data in the probability distribution for the likelihood function. Hence, all of the PDFs given above were renormalized to account for this missing data by dividing by the factor F, where t_o is the cutoff time below which all events are missed (~0.2 ms for 1-kHz Bessel filtering):

$$F = \int_{t_o}^{\infty} p(t \mid \theta)dt = \sum_i a_i e^{-t_0/\tau_i}, \tag{A9}$$

where the sum is over all exponential components.

Degenerate likelihood and priors

As described in the main text, the rate constants c, d, and z for the Ba^{2+} blocks are underdetermined by the internal Ba^{2+} experiments, as there are only two exponentials measured with three experimentally accessible unknowns: two time constants and one amplitude. This state of affairs renders the likelihood function for the Ba^{2+} blocks degenerate and in practice means that many different combinations of c, d, and z are all consistent with the data, although to differing degrees. Fortunately, Bayesian methods provide workable solutions to underdetermined problems as long as proper priors are used, although degenerate likelihoods usually result in wide posterior distributions for the parameters. For this reason, we used informative, though vague, priors for c, d, and z in the analyses of internal Ba^{2+} data. The sum of two of the eigenvalues of the blocking scheme has a simple analytic relationship to the rate constants (Eq. 4c in the main text):

$$\frac{1}{\tau_f} + \frac{1}{\tau_s} = b + c + d + z. \tag{A10}$$

From previous experimental work with internal Ba^{2+} blocks, we know that the sum of these two eigenvalues is roughly 300 s^{-1}. Hence, we conservatively assume vague exponential (maximum entropy) priors for b, c, d, and z, each with a mean of 100 s^{-1}. Conventional reference priors (Lee, 2004) were used for all other rate constants (i.e., the inverse of the rate constant).

With external Ba^{2+}, z is fully identified by the sum of the block-time amplitudes $a_f + a_s$, according to (Eq. 6) in the main text. In a separate analysis, we therefore used the posterior distribution of z from external Ba^{2+} data as a proper data-based prior for z with the internal Ba^{2+} data. This procedure effectively turns an underdetermined problem into a determined one. For convenience, we approximated the posterior distribution for z from the external Ba^{2+} analyses as a gamma distribution characterized by the mean and variance of the posterior.

Metropolis-coupled Markov chain Monte Carlo algorithm and posterior analysis

Posterior distributions of the parameters were approximated using a parallel Metropolis-coupled Markov chain Monte Carlo algorithm (Metropolis et al., 1953; Hastings, 1970; Geyer, C.J. 1991. Markov chain Monte Carlo maximum likelihood. Computing Science and Statistics Proceedings of the 23rd Symposium on the Interface; Green, 1995; Altekar et al., 2004). Because the posterior distribution dictated by the likelihood function (Eq. A3) and our assumed priors has no analytic form, we used Metropolis–Hastings moves to generate samples from the posterior distribution. Eight chains (two cold and six heated) were run in parallel using the Metropolis-coupled algorithm to efficiently explore the multimodal parameter space. Chains were generally run for one million iterations, sampling every 100 iterations. Convergence was assessed by monitoring the potential scale reduction factor statistic (Gelman, 2004) and requiring that it drop below 1.01. The first half of the iterations were discarded as "burn-in." The joint posterior distribution of the parameters was investigated and

summarized by histogram and moment analysis. Analysis of a single parameter from the joint posterior distribution samples provides an approximation of the marginal posterior distribution for that parameter.

Appendix B

High-resolution measurement of K^+/Na^+ selectivity of KcsA-E71A by reversal potential

Reversal potential measurements of selectivity under strictly bi-ionic conditions (K^+ only intracellular, Na^+ only extracellular) are usually impossible for K^+ channels, as no Na^+ current is observed even at very negative voltage, and so no reversal can be interpolated in the I-V plot. The present measurement seeks to determine K^+/Na^+ selectivity under "almost bi-ionic" conditions, with a large but well-defined K^+ gradient and Na^+ on only the external side of the channel. (These experiments use internal solution of 200 mM K^+ and external solution of 10 mM K^+ plus 190 mM Na^+.) The reversal potential of the single-channel I-V curve, V_c, is then compared with the reversal potential, V_K, of an ideally K^+-selective ionophore, valinomycin, added to the planar bilayer immediately after the single-channel measurement. The difference between these two reversal potentials, $\Delta V = V_c - V_K$, nulls out small electrical imbalances and uncertainties regarding single-ion activity coefficients, and thereby determines the channel reversal potential with uncertainties on the order of 1 mV (Miller, 1987; LeMasurier et al., 2001). It may be easily shown that:

$$\frac{P_{Na}}{P_K} = \frac{F\Delta V}{RT} \cdot \frac{[K^+]_{ex}}{[Na^+]_{ex}} \sim \frac{\Delta V}{475} \qquad \text{(B1)}$$

under our conditions, where ΔV is in millivolts and T = 21°C.

Analysis of four independent KcsA-E71A KcsA datasets resulted in $\Delta V = -0.8 \pm 1.3$ mV, showing that E71A-KcsA and valinomycin cannot be distinguished in K^+/Na^+ selectivity by reversal potential under these conditions. This does not mean, however, that the KcsA mutant's selectivity is identical to the nearly perfect K^+ selectivity of valinomycin. The uncertainty in these measurements places a lower limit (based on a 2-σ limit) of $P_K/P_{Na} > \sim 250$. This lower limit is similar to that found for wild-type KcsA by this method (LeMasurier et al., 2001).

We are grateful for the copious ridicule and humiliation supplied by Miller laboratory members and Dr. C. Darwin upon scrutinizing drafts of the manuscript.

Frederick J. Sigworth served as guest editor.

Submitted: 28 June 2011
Accepted: 22 August 2011

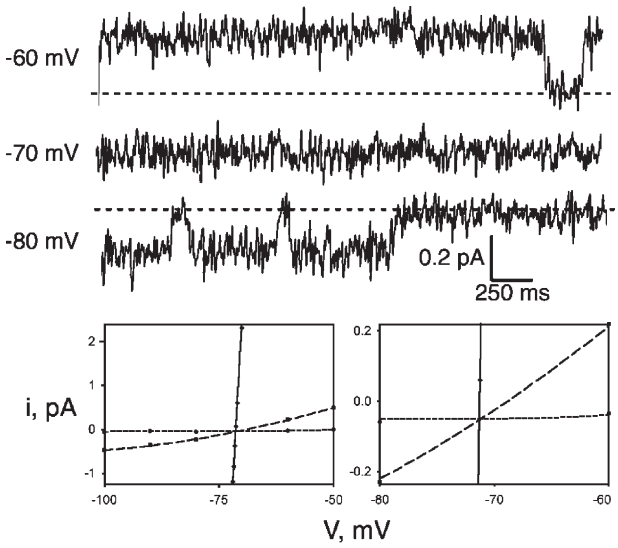

Figure B1. Single KcsA-E71A channels were recorded as in the main text, with 200 mM K^+ in/10 mM K^+ and 190 mM Na^+ out. 10 µM Ba^{2+} was also included in the internal solution to produce block events. Immediately after recording a single-channel I-V curve, 25 µM valinomycin was added to the bilayer to raise the conductance ~100-fold, and the macroscopic I-V curve was measured within a minute. (Top) Illustrative records (filtered at 50 Hz) at voltages on either side of the reversal potential before the addition of valinomycin. Dashed line marks zero-current level. (Bottom) I-V curves for open channel (squares), blocked channel (circles), and valinomycin (diamonds). Curves (dashed for channel, solid for valinomycin) are third-order polynomial fits to the data points. Reversal potential is the voltage at which the open-channel or valinomycin curve crosses the blocked-channel curve. Right panel is a blown-up view of left panel.

REFERENCES

Altekar, G., S. Dwarkadas, J.P. Huelsenbeck, and F. Ronquist. 2004. Parallel Metropolis coupled Markov chain Monte Carlo for Bayesian phylogenetic inference. *Bioinformatics.* 20:407–415. http://dx.doi.org/10.1093/bioinformatics/btg427

Andersen, O.S. 2011. Perspectives on: ion selectivity. *J. Gen. Physiol.* 137:393–395. http://dx.doi.org/10.1085/jgp.201110651

Åqvist, J., and V. Luzhkov. 2000. Ion permeation mechanism of the potassium channel. *Nature.* 404:881–884. http://dx.doi.org/10.1038/35009114

Baukrowitz, T., and G. Yellen. 1996. Use-dependent blockers and exit rate of the last ion from the multi-ion pore of a K^+ channel. *Science.* 271:653–656. http://dx.doi.org/10.1126/science.271.5249.653

Bernardo, J.M., and A.F.M. Smith. 1994 Bayesian Theory. Wiley, Chichester, England. 586 pp.

Bernèche, S., and B. Roux. 2001. Energetics of ion conduction through the K^+ channel. *Nature.* 414:73–77. http://dx.doi.org/10.1038/35102067

Bezanilla, F., and C.M. Armstrong. 1972. Negative conductance caused by entry of sodium and cesium ions into the potassium channels of squid axons. *J. Gen. Physiol.* 60:588–608. http://dx.doi.org/10.1085/jgp.60.5.588

Bhate, M.P., B.J. Wylie, L. Tian, and A.E. McDermott. 2010. Conformational dynamics in the selectivity filter of KcsA in response to potassium ion concentration. *J. Mol. Biol.* 401:155–166. http://dx.doi.org/10.1016/j.jmb.2010.06.031

Chakrapani, S., J.F. Cordero-Morales, V. Jogini, A.C. Pan, D.M. Cortes, B. Roux, and E. Perozo. 2011. On the structural basis of

modal gating behavior in K(+) channels. *Nat. Struct. Mol. Biol.* 18:67–74. http://dx.doi.org/10.1038/nsmb.1968

Cheng, W.W., J.G. McCoy, A.N. Thompson, C.G. Nichols, and C.M. Nimigean. 2011. Mechanism for selectivity-inactivation coupling in KcsA potassium channels. *Proc. Natl. Acad. Sci. USA.* 108:5272–5277. http://dx.doi.org/10.1073/pnas.1014186108

Colquhoun, D., and A.G. Hawkes. 2009a. The principles of the stochastic interpretation of ion-channel mechanisms. *In* Single-Channel Recording. B. Sakmann and E. Neher, editors. Springer, New York. 397–482.

Colquhoun, D., and A.G. Hawkes. 2009b. A Q-matrix cookbook: how to write only one program to calculate the single-channel and macroscopic predictions for any kinetic mechanism. *In* Single-Channel Recording. B. Sakmann and E. Neher, editors. Springer, New York. 589–633.

Cordero-Morales, J.F., L.G. Cuello, Y. Zhao, V. Jogini, D.M. Cortes, B. Roux, and E. Perozo. 2006. Molecular determinants of gating at the potassium-channel selectivity filter. *Nat. Struct. Mol. Biol.* 13:311–318. http://dx.doi.org/10.1038/nsmb1069

Csanády, L., P. Vergani, and D.C. Gadsby. 2010. Strict coupling between CFTR's catalytic cycle and gating of its Cl^- ion pore revealed by distributions of open channel burst durations. *Proc. Natl. Acad. Sci. USA.* 107:1241–1246. http://dx.doi.org/10.1073/pnas.0911061107

Derebe, M.G., D.B. Sauer, W. Zeng, A. Alam, N. Shi, and Y. Jiang. 2011. Tuning the ion selectivity of tetrameric cation channels by changing the number of ion binding sites. *Proc. Natl. Acad. Sci. USA.* 108:598–602. http://dx.doi.org/10.1073/pnas.1013636108

Doyle, D.A., J. Morais Cabral, R.A. Pfuetzner, A. Kuo, J.M. Gulbis, S.L. Cohen, B.T. Chait, and R. MacKinnon. 1998. The structure of the potassium channel: molecular basis of K^+ conduction and selectivity. *Science.* 280:69–77. http://dx.doi.org/10.1126/science.280.5360.69

Egwolf, B., and B. Roux. 2010. Ion selectivity of the KcsA channel: a perspective from multi-ion free energy landscapes. *J. Mol. Biol.* 401:831–842. http://dx.doi.org/10.1016/j.jmb.2010.07.006

Gao, L., X. Mi, V. Paajanen, K. Wang, and Z. Fan. 2005. Activation-coupled inactivation in the bacterial potassium channel KcsA. *Proc. Natl. Acad. Sci. USA.* 102:17630–17635. http://dx.doi.org/10.1073/pnas.0505158102

Gelman, A. 2004. Bayesian Data Analysis. Chapman and Hall/CRC, Boca Raton, FL. 696 pp.

Gin, E., M. Falcke, L.E. Wagner, D.I. Yule, and J. Sneyd. 2009. Markov chain Monte Carlo fitting of single-channel data from inositol trisphosphate receptors. *J. Theor. Biol.* 257:460–474. http://dx.doi.org/10.1016/j.jtbi.2008.12.020

Green, P.J. 1995. Reversible jump Markov chain Monte Carlo computation and Bayesian model determination. *Biometrika.* 82:711–732. http://dx.doi.org/10.1093/biomet/82.4.711

Harris, R.E., H.P. Larsson, and E.Y. Isacoff. 1998. A permanent ion binding site located between two gates of the *Shaker* K^+ channel. *Biophys. J.* 74:1808–1820. http://dx.doi.org/10.1016/S0006-3495(98)77891-9

Hastings, W.K. 1970. Monte Carlo sampling methods using Markov chains and their applications. *Biometrika.* 57:97–109. http://dx.doi.org/10.1093/biomet/57.1.97

Heginbotham, L., M. LeMasurier, L. Kolmakova-Partensky, and C. Miller. 1999. Single *Streptomyces lividans* K^+ channels: functional asymmetries and sidedness of proton activation. *J. Gen. Physiol.* 114:551–560. http://dx.doi.org/10.1085/jgp.114.4.551

Hille, B. 2001. Ion Channels of Excitable Membranes. Third edition. Sinauer Associates, Sunderland, MA. 814 pp.

Hille, B., and W. Schwarz. 1978. Potassium channels as multi-ion single-file pores. *J. Gen. Physiol.* 72:409–442. http://dx.doi.org/10.1085/jgp.72.4.409

Hodgkin, A.L., and R.D. Keynes. 1955. The potassium permeability of a giant nerve fibre. *J. Physiol.* 128:61–88.

Kijima, S., and H. Kijima. 1987. Statistical analysis of channel current from a membrane patch. I. Some stochastic properties of ion channels or molecular systems in equilibrium. *J. Theor. Biol.* 128:423–434. http://dx.doi.org/10.1016/S0022-5193(87)80188-1

Lee, P.M. 2004. Bayesian Statistics: An Introduction. Third edition. Arnold, London. 351 pp.

LeMasurier, M., L. Heginbotham, and C. Miller. 2001. KcsA: it's a potassium channel. *J. Gen. Physiol.* 118:303–314. http://dx.doi.org/10.1085/jgp.118.3.303

Levitt, D.G. 1978. Electrostatic calculations for an ion channel. I. Energy and potential profiles and interactions between ions. *Biophys. J.* 22:209–219. http://dx.doi.org/10.1016/S0006-3495(78)85485-X

Lockless, S.W., M. Zhou, and R. MacKinnon. 2007. Structural and thermodynamic properties of selective ion binding in a K^+ channel. *PLoS Biol.* 5:e121. http://dx.doi.org/10.1371/journal.pbio.0050121

Metropolis, N., A.W. Rosenbluth, M.N. Rosenbluth, A.H. Teller, and E. Teller. 1953. Equations of state calculations by fast computing machines. *J. Chem. Phys.* 21:1087–1091. http://dx.doi.org/10.1063/1.1699114

Miller, C. 1987. Trapping single ions inside single ion channels. *Biophys. J.* 52:123–126. http://dx.doi.org/10.1016/S0006-3495(87)83196-X

Morais-Cabral, J.H., Y. Zhou, and R. MacKinnon. 2001. Energetic optimization of ion conduction rate by the K^+ selectivity filter. *Nature.* 414:37–42. http://dx.doi.org/10.1038/35102000

Neyton, J., and C. Miller. 1988a. Discrete Ba^{2+} block as a probe of ion occupancy and pore structure in the high-conductance Ca^{2+}-activated K^+ channel. *J. Gen. Physiol.* 92:569–586. http://dx.doi.org/10.1085/jgp.92.5.569

Neyton, J., and C. Miller. 1988b. Potassium blocks barium permeation through a calcium-activated potassium channel. *J. Gen. Physiol.* 92:549–567. http://dx.doi.org/10.1085/jgp.92.5.549

Noskov, S.Y., and B. Roux. 2007. Importance of hydration and dynamics on the selectivity of the KcsA and NaK channels. *J. Gen. Physiol.* 129:135–143. http://dx.doi.org/10.1085/jgp.200609633

Noskov, S.Y., S. Bernèche, and B. Roux. 2004. Control of ion selectivity in potassium channels by electrostatic and dynamic properties of carbonyl ligands. *Nature.* 431:830–834. http://dx.doi.org/10.1038/nature02943

Rosales, R.A. 2004. MCMC for hidden Markov models incorporating aggregation of states and filtering. *Bull. Math. Biol.* 66:1173–1199. http://dx.doi.org/10.1016/j.bulm.2003.12.001

Roux, B. 2010. Exploring the ion selectivity properties of a large number of simplified binding site models. *Biophys. J.* 98:2877–2885. http://dx.doi.org/10.1016/j.bpj.2010.03.038

Siekmann, I., L.E. Wagner II, D. Yule, C. Fox, D. Bryant, E.J. Crampin, and J. Sneyd. 2011. MCMC estimation of Markov models for ion channels. *Biophys. J.* 100:1919–1929. http://dx.doi.org/10.1016/j.bpj.2011.02.059

Sohma, Y., A. Harris, C.J. Wardle, B.E. Argent, and M.A. Gray. 1996. Two barium binding sites on a maxi K^+ channel from human vas deferens epithelial cells. *Biophys. J.* 70:1316–1325. http://dx.doi.org/10.1016/S0006-3495(96)79688-1

Thompson, A.N., D.J. Posson, P.V. Parsa, and C.M. Nimigean. 2008. Molecular mechanism of pH sensing in KcsA potassium channels. *Proc. Natl. Acad. Sci. USA.* 105:6900–6905. http://dx.doi.org/10.1073/pnas.0800873105

Thompson, A.N., I. Kim, T.D. Panosian, T.M. Iverson, T.W. Allen, and C.M. Nimigean. 2009. Mechanism of potassium-channel selectivity revealed by Na^+ and Li^+ binding sites within the

KcsA pore. *Nat. Struct. Mol. Biol.* 16:1317–1324. http://dx.doi.org/10.1038/nsmb.1703

Varma, S., D. Sabo, and S.B. Rempe. 2008. K^+/Na^+ selectivity in K channels and valinomycin: over-coordination versus cavity-size constraints. *J. Mol. Biol.* 376:13–22. http://dx.doi.org/10.1016/j.jmb.2007.11.059

Vergara, C., and R. Latorre. 1983. Kinetics of Ca^{2+}-activated K^+ channels from rabbit muscle incorporated into planar bilayers. Evidence for a Ca^{2+} and Ba^{2+} blockade. *J. Gen. Physiol.* 82:543–568. http://dx.doi.org/10.1085/jgp.82.4.543

Vergara, C., O. Alvarez, and R. Latorre. 1999. Localization of the K^+ lock-in and the Ba^{2+} binding sites in a voltage-gated calcium-modulated channel. Implications for survival of K^+ permeability. *J. Gen. Physiol.* 114:365–376. http://dx.doi.org/10.1085/jgp.114.3.365

Ye, S., Y. Li, and Y. Jiang. 2010. Novel insights into K^+ selectivity from high-resolution structures of an open K+ channel pore. *Nat. Struct. Mol. Biol.* 17:1019–1023. http://dx.doi.org/10.1038/nsmb.1865

Zhou, Y., and R. MacKinnon. 2003. The occupancy of ions in the K^+ selectivity filter: charge balance and coupling of ion binding to a protein conformational change underlie high conduction rates. *J. Mol. Biol.* 333:965–975. http://dx.doi.org/10.1016/j.jmb.2003.09.022